Supporting Information

Combining multi-band slice selection with consistent k-t-space EPSI for accelerated spectral imaging

Rita Schmidt[1,2], Amir Seginer[3], Assaf Tal[3]*

[1]*Department of Neurobiology, Weizmann Institute of Science, Rehovot, Israel*

[2]*Radiology, Leiden University Medical Center, Leiden, Netherlands*

[3]*Department of Chemical and Biological physics, Weizmann Institute of Science, Rehovot, Israel*

Table S1. Comparison of the SNR of variant I and II (in Figure 3), each relative to EPSI (as a reference).

	Water SNR ratio	NAA SNR ratio	NAA SNR/√t ratio
EPSI (Fig1a,odd+even)	1 (Reference)	1 (Reference)	1 (Reference)
Variant I (Fig.1b)	1.01±0.004	1.005±0.005	1.005±0.005
EPSI (Fig1.a, odd only)	0.709±0.002	0.706±0.003	0.706±0.003
Variant II (Fig.1c)	0.702±0.002	0.700±0.003	0.99±0.004

Dual-band CAIPIRINHA consistent k-t space EPSI - g-factor analysis

In order to analyze the dual-band CAIPIRINHA implementation, we examined the geometry factor (g-factor) maps for two setups that includes two different FOV and object dimensions. The g-factor maps for multi-band are defined as the ratio of the $SNR_{accelerated}/SNR_{full}$ and can be calculated using the sensitivity maps. In addition, we examined the reconstruction of the details in a high-resolution ACR phantom for variant III, comparing simultaneous acquisition of adjacent and unadjacent slices (Fig. S1). g-factor maps of the two examined setups reach up to 5% deviation in the first setup and up

to 20% for the second setup. No difference is observed between the g-factor maps for excitation of adjacent and not adjacent slices. The details of the high-resolution ACR phantom are well reconstructed for all cases.

1. Kellman, P., & McVeigh, E. R. (2005). Image reconstruction in SNR units: a general method for SNR measurement. *Magnetic Resonance in Medicine*, *54*(6), 1439–1447.

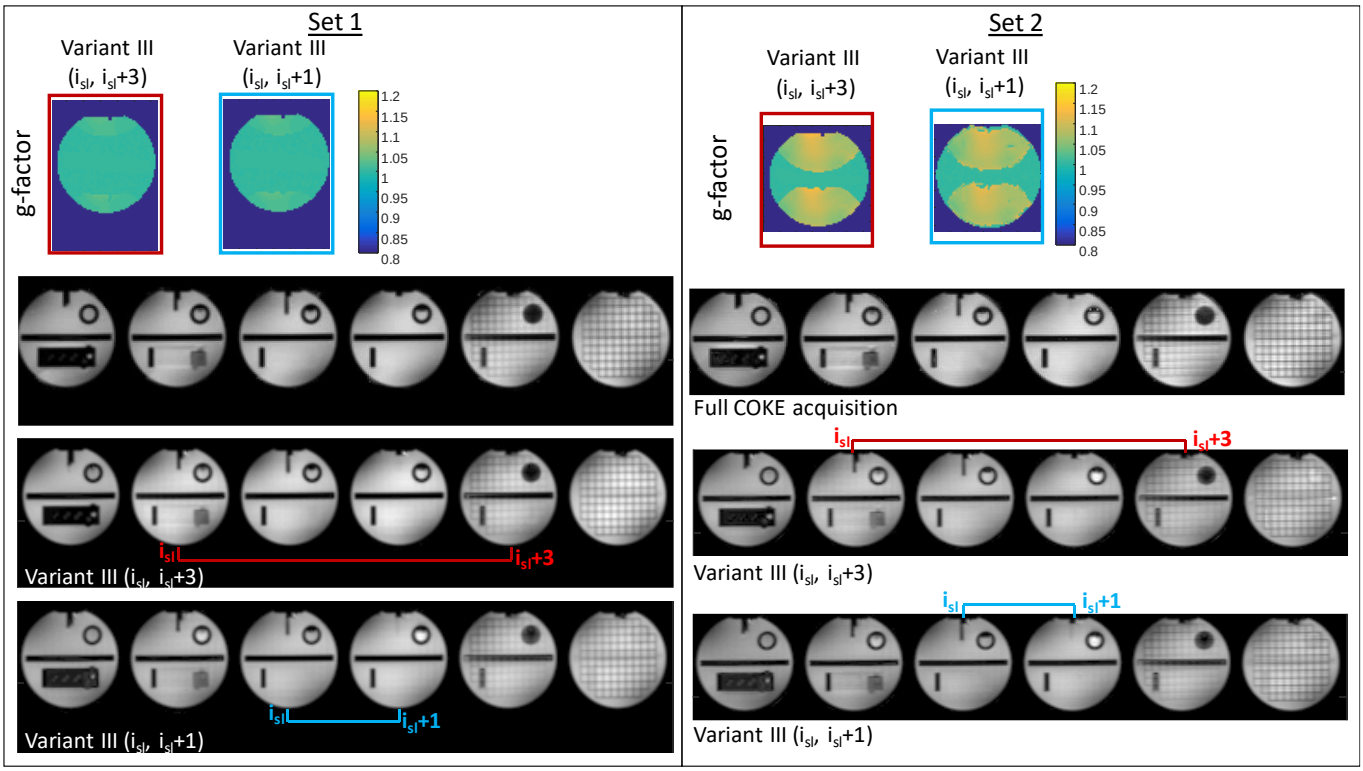

Figure S1. Dual-band CAIPIRINHA variant III - g-factor maps and high resolution ACR phantom reconstruction of simultaneous excitation of adjacent (i_{sl}, i_{sl}+1) and not adjacent (i_{sl}, i_{sl}+3) slices. Set 1 and Set 2 examples show two different FOV and object dimensions. The scan parameters for set 1 were: TR/TE 1500/15 ms, FOV and thickness 270x192x8 mm^3, in-plane resolution 3x3 mm^2, SW =1000 Hz, for set 2: FOV and thickness 192x192x8 mm^3, in-plane resolution 3x3 mm^2, SW =1000 Hz.

Schematic illustration of the lipid ghost in case of a dual-band CAIPIRINHA – adjacent compared to non-adjacent slices

As was demonstrated in the manuscript, remaining ghost artifacts still can be present in the consistent k-t space EPSI. In case of a dual-band CAIPIRINHA excitation, these ghosts occur for each of the slices in a shifted manner similarly to the real slice information.

Although the ghost intensity is about 4-5%, the lipid's ghost contribution can be significant. The schematic illustration below shows that for dual-band CAIPIRINHA excitation, exciting adjacent slices - due to their similarity in the lipid location - can keep the lipid artifacts in the lipid's region. Obviously, it does not mean that the artifact's signal is lower, but it is located in the region that has lower impact if one is interested in the metabolites information in the brain.

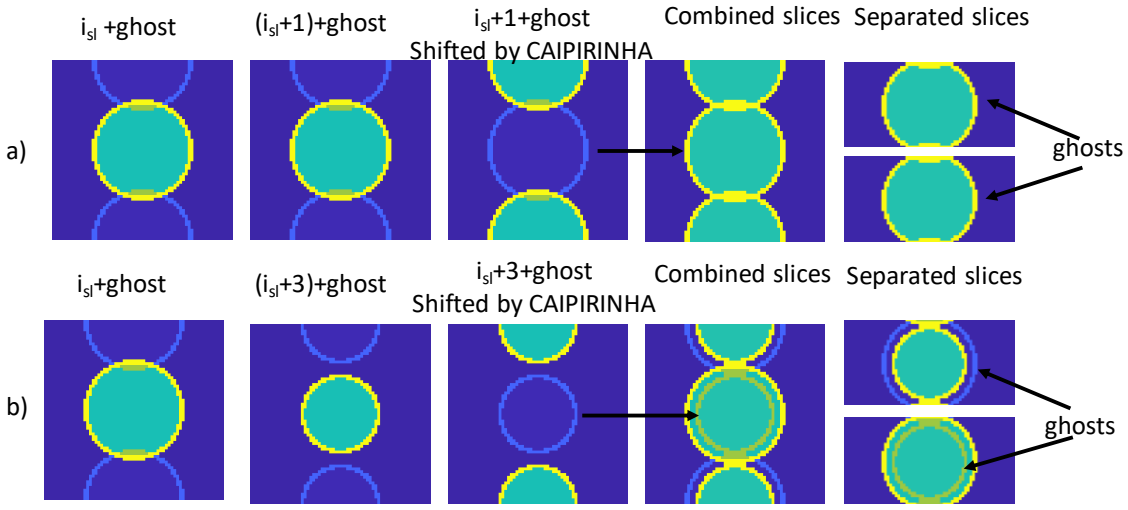

Figure S2. Schematic illustration of the ghost artifacts for dual-band CAIPIRINHA case with adjacent (i_{sl}, i_{sl}+1) and not adjacent (i_{sl}, i_{sl}+3) slices, shown in a) and b) respectively. The simulation shows a spherical-shape phantom with signal inside mimicking metabolites equal to one and a ring mimicking lipid 10x higher. The ghost is simulated having 4% from the original signal. The adjacent slices have the same radius and the non-adjacent slices have different radius. The scale of the images is from 0 to 2.

Complementary results of the in-vivo experiment

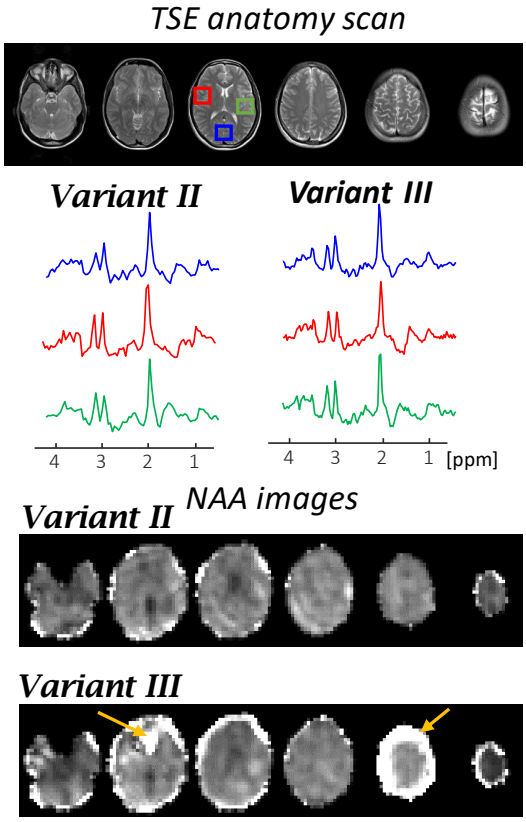

Figure S3. In-vivo results of variants II and III. From top to bottom: TSE anatomy images of the scanned slices; real spectra for each MRSI method at three regions (each averaging over 5x5 voxels) in the central slice (shown in red, blue and green rectangle overlays); and images of six slices for NAA using spectra integration in the range of 0.4 ppm. The image intensities of NAA is normalized to the NAA intensity in each of the methods.

Creatine and Choline images for the in-vivo example from Figure 5

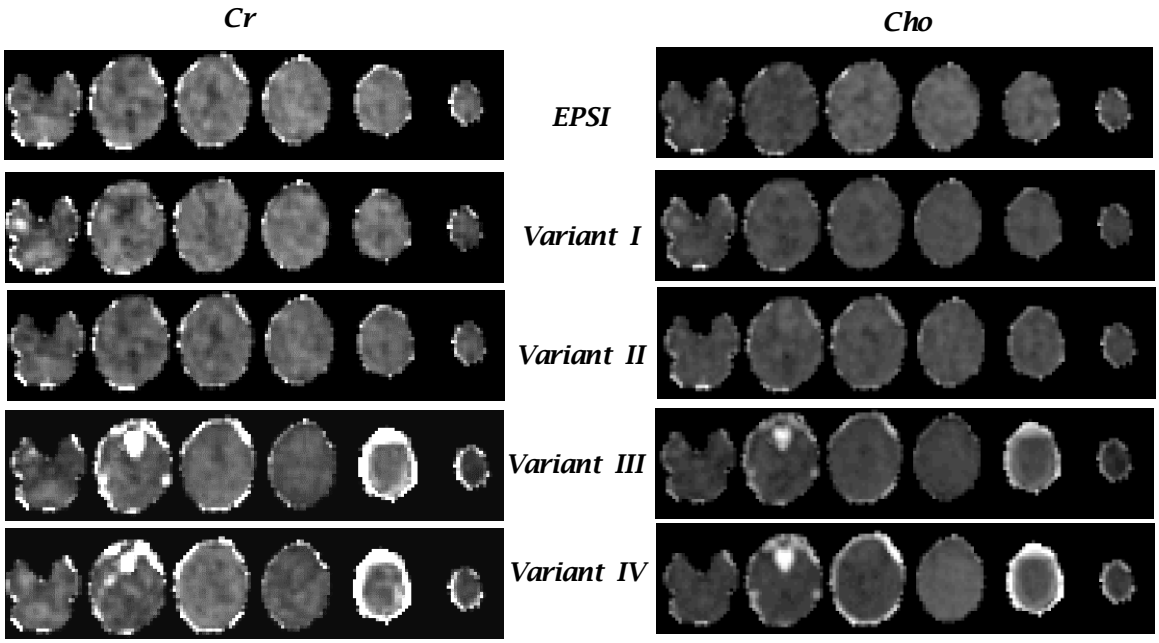

Figure S4. Creatine and Choline images of the in-vivo results of EPSI and variants I-IV acquisitions. Images of six slices are shown for each of the methods.

LCmodel fitted results

The following figure shows the NAA/tCr ratio maps estimated by the LCModel fitting. The spectra were fitted in the range of 0.2 to 4.2 ppm. The basis-set was simulated using MATLAB code including 17 metabolites (Ala, Asp, Cr, PCr, GABA, Glc, Gln, Glu, GSH, GPC, PCho, Lac, mI, NAA, NAAG, sI, Tau) with a linewidth of 8 Hz. The resulting images were thresholded to show pixels with estimated standard deviations (CRLB) <100%. The average standard deviations for all slices of each scan (EPSI, variants I-IV, respectively) were 44%, 36%, 47%, 40% and 40%.

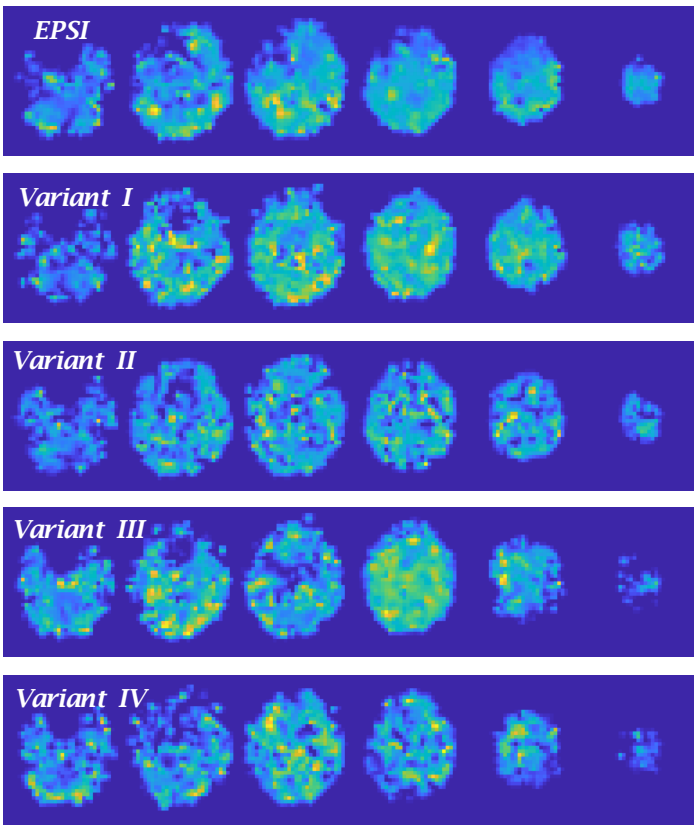

Figure S5. NAA/tCr ratio maps estimated by the LCModel fitting for EPSI and variant I-IV.

In-vivo single voxel spectra

The following figure show the spectra of a single voxel in the center of the blue ROI from Figure 5.

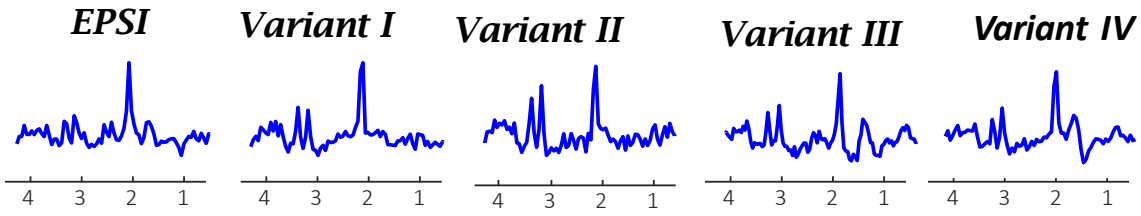

Figure S6. Single voxel spectra for each MRSI method at the blue ROI (central voxel) – EPSI and variants I-IV, respectively.

Ghosts' artifact in dual-band CAIPIRINHA variant III in the in-vivo example from Figure 5

In the current study, we showed that the residual ghost intensity in consistent k-t space EPSI due to PE inconsistencies is within 5%. When consistent k-t space EPSI is combined with dual-band CAIPIRINHA, the ghost artifact will also lead to lipid contamination, as in the upper slices of the in-vivo example in Fig. 5. Note that a ghost artifact of up to 5% due to lipid contamination and water sidebands - which can occur due to B_0 inhomogeneity - is still relatively high signal compared to the metabolites. Figure S7 summarizes the resulting ghost artifact induced by employing dual-band CAIPIRINHA acceleration in variant III for the in-vivo data (Fig. 5).

The ratio of the NAA images of dual-band CAIPIRINHA variant III and variant I was taken at each point and a histogram of the values was generated. We fit a Gaussian to this histogram based on all values left of the peak (see Figure S7). A threshold of 2σ (>95%, σ- the Gaussian RMS width) was used to estimate the voxels that represent possible artifacts due to lipid contamination. This threshold corresponds to a ratio of 1.35. The resulting fit is shown in Fig. S7b. Intensities with a ratio above 1.35 are also shown with a red overlay in Fig. S7a. The above estimation resulted in 26% of the total number of voxels marked as an artifact. However, it can be seen that the central slices have negligible artifacts, and that most artifacts appear in the superior slices, which have very high lipid content. Another possible reason for the increased lipid contamination is the high angle the skull makes through the imaging plane. The average value of the intensities ratio (excluding the lipids artifacts) is 0.92 ± 0.19, which is reasonable taking into account the g-factor maps in Fig. S1.

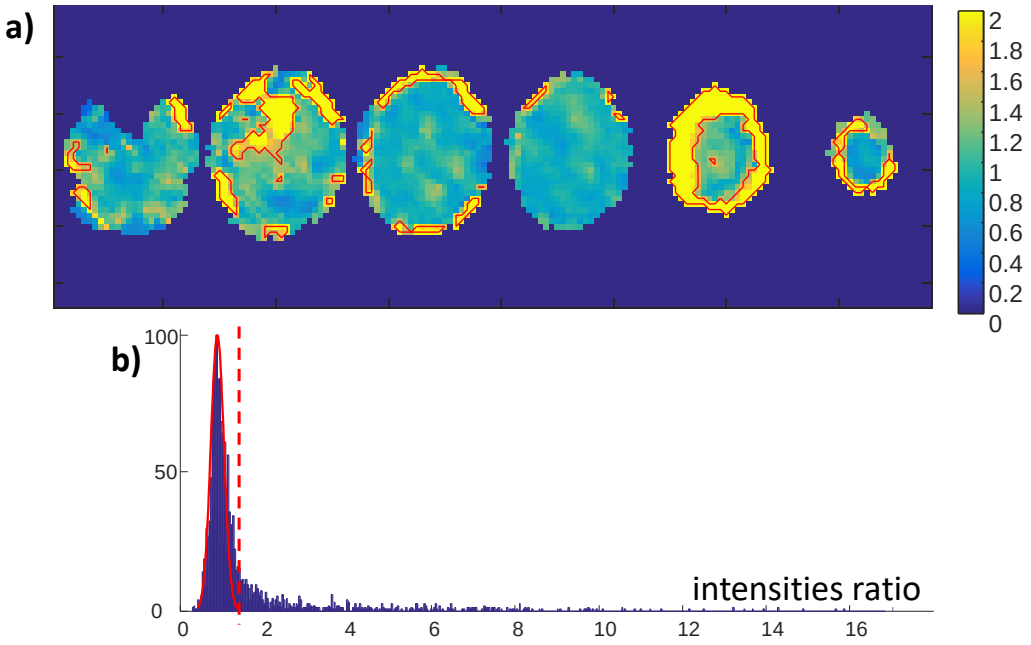

Figure S7. Lipid contamination estimation dual-band CAIPIRINHA variant III compared to variant I (in-vivo example from Fig.5). a) Ratio of the NAA images dual-band CAIPIRINHA variant III and variant I. b) histogram of the ratio values in a).